ORIGINAL ARTICLE

Numerical simulation of long-duration blast wave evolution in confined facilities

F. Togashi · J. D. Baum · E. Mestreau · R. Löhner · D. Sunshine

Abstract The objective of this research effort was to investigate the quasi-steady flow field produced by explosives in confined facilities. In this effort we modeled tests in which a high explosive (HE) cylindrical charge was hung in the center of a room and detonated. The HEs used for the tests were C-4 and AFX 757. While C-4 is just slightly under-oxidized and is typically modeled as an ideal explosive, AFX 757 includes a significant percentage of aluminum particles, so long-time afterburning and energy release must be considered. The Lawrence Livermore National Laboratory (LLNL)-produced thermo-chemical equilibrium algorithm, "Cheetah", was used to estimate the remaining burnable detonation products. From these remaining species, the afterburning energy was computed and added to the flow field. Computations of the detonation and afterburn of two HEs in the confined multi-room facility were performed. The results demonstrate excellent agreement with available experimental data in terms of blast wave time of arrival, peak shock amplitude, reverberation, and total impulse (and hence, total energy release, via either the detonation or afterburn processes.

Communicated by C. Needham.

F. Togashi (✉) · J. D. Baum · E. Mestreau
SAIC, Technology and Advanced Systems,
1710 SAIC Dr. MS 2-6-9, McLean, USA
e-mail: fumiya.togashi@saic.com

R. Löhner
College of Science, George Mason University,
4400 University Dr., Fairfax, VA 22030, USA

D. Sunshine
TDSH, Defense Threat Reduction Agency,
Fort Belvoir, VA 22060, USA

1 Introduction

The numerical analysis of solid explosives can be performed similar to gaseous detonations, by applying the proper equation of state (EOS) applicable to the high-pressure and high-temperature conditions of the Chapman–Jouguet theory. Nevertheless, unlike gaseous detonation, solid HEs are generally composed of compressed explosive, binder, and plasticizer that include voids even when density is close to the theoretical maximum density. These heterogeneous explosives behave differently from gaseous detonations, as chemical reaction in the detonation front is not always in equilibrium.

One of the famous often-used EOS applied to the modeling of solid explosives is the Jones–Wilkins–Lee (JWL) model [1]. The JWL–EOS is used to define the principle adiabat that corresponds to the steady-state expansion of the reaction products. The JWL parameter set is obtained by parameter fitting to the relationship between pressure and co-volume from the experiment. The model is very useful to evaluate the peak pressure of the shock arrival and the impulse for a short period. However, the reliability of its thermo-dynamical compatibility is unclear so that it is not suitable for the analysis of a long-term blast wave which has to consider long-time energy release (the so called afterburning effect). Consider TNT ($C_7H_5N_3O_6$), which is a significantly under-oxidized explosive. Its overall reaction is [2]: $C_7H_5N_2O_6 \rightarrow 1.5N_2 + 2.5H_2O + 3.5CO + 3.5C$.

After detonation is completed, the remaining gaseous C and CO at high temperature are mixed in air and are capable of interacting to produce CO_2. Both Schwer et al. [3]

Fig. 1 Test facility and pressure gauge locations
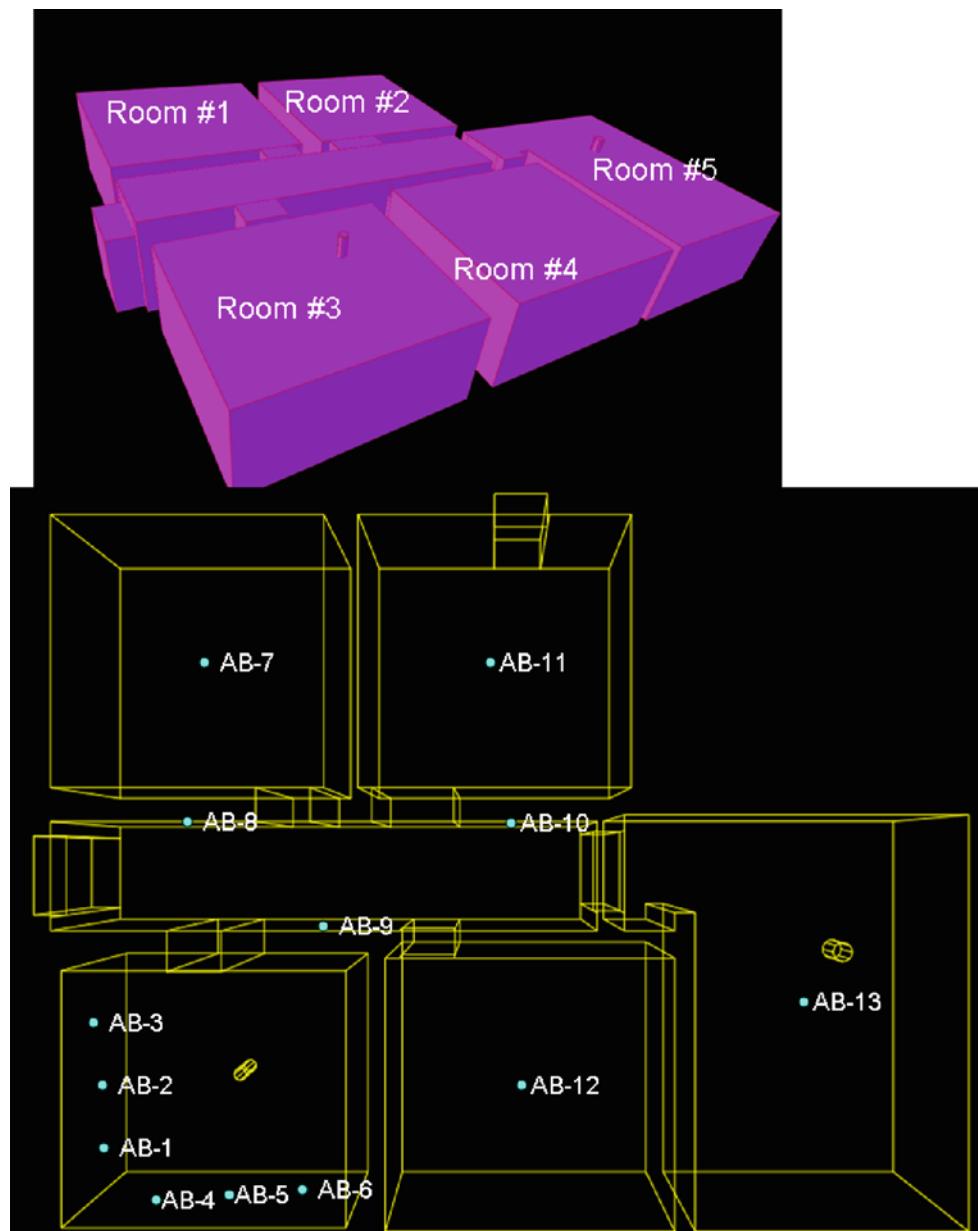
and Kuhl et al. [4] have reported significant afterburn energy release for TNT detonation modeling.

In contrast, past experience with C-4 had indicated a relatively insignificant amount of afterburn energy addition for either open environment, or confined room, at least for relatively short time. C-4 is composed of 91% RDX ($C_3H_6N_6O_6$) and 9% of binders such as DOP ($H_{38}C_{24}O_4$), PIB (H_8C_4), and fuel-oil [2]. Compared with TNT, the oxygen balance of RDX is relatively higher. Nevertheless, as C-4 is under-oxidized, it is possible to gain afterburning energy for long-term blast wave evolution in confined rooms.

Another explosive, AFX757, was analyzed, which contains 33% Al particles, and produces Alumina after deto-

nation completion. Aluminum particles are often used in explosives and solid propellant to increase energy release. The Al particle combustion time under these conditions is significantly higher than detonation time and is capable of burning behind the detonation front. Hence, energy release after detonation front passage (afterburning) is inevitable to the accurate modeling of Aluminized explosives.

The main objective of this study is to investigate C-4 long-term blast wave evolution and afterburning in a confined environment, and to establish a reasonable numerical model (i.e., without resorting to expensive CPU calculations of first-principles reaction models) for estimating afterburning effect of long-term blast wave evolution in confined environments.

Fig. 2 **a** Gouraud shading of absolute velocity and detonation product fraction at 0.5 ms. **b** Gouraud shading of absolute velocity and detonation product fraction at 5.4 ms. **c** Gouraud shading of absolute velocity and detonation product fraction at 10 ms. **d** Gouraud shading of absolute velocity and detonation product fraction at 18 ms. **e** Gouraud shading of absolute velocity and detonation product fraction at 30 ms. **f** Gouraud shading of absolute velocity and detonation product fraction at 40 ms. **g** Gouraud shading of absolute velocity and detonation product fraction at 55 ms. **h** Gouraud shading of absolute velocity and detonation product fraction at 90 ms
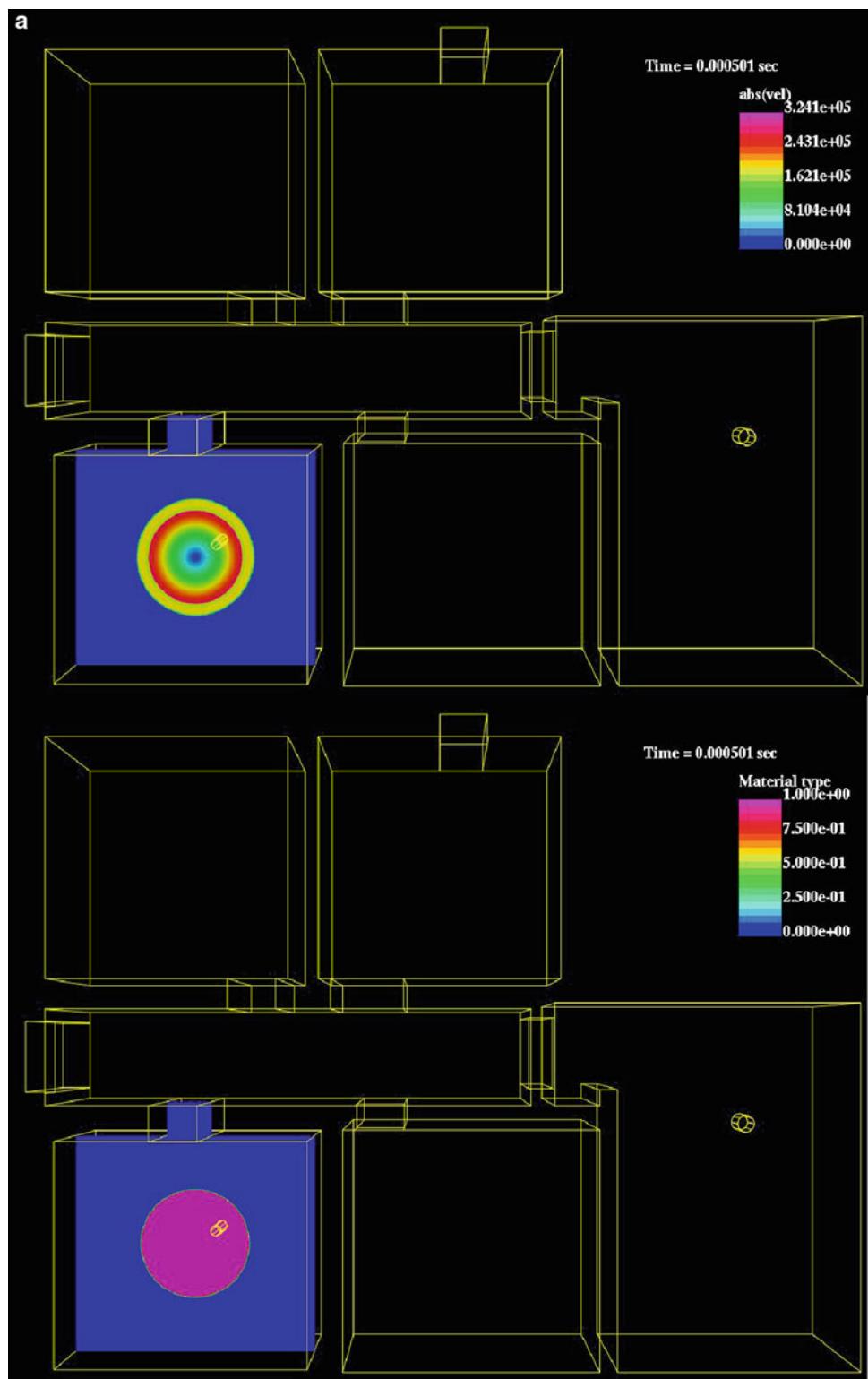

2 Flow solver

The numerical simulation was done by FEFLO, a general-purpose Computational Fluid Dynamics (CFD) code based on the following general principles:

– Use of unstructured grids (automatic grid generation and mesh refinement);
– Finite element discretization of space;
– Separate flow modules for compressible and incompressible flows;

Fig. 2 continued
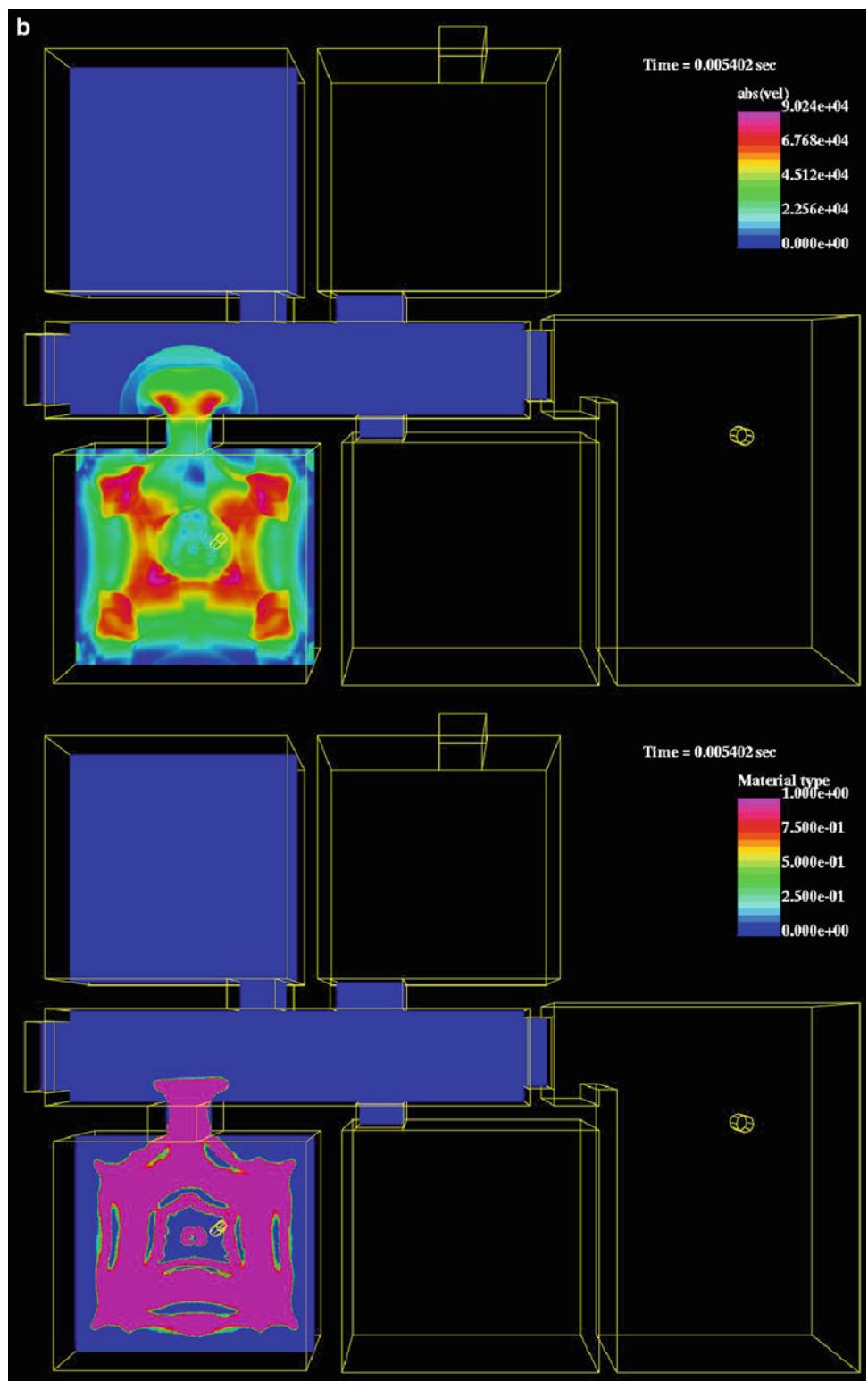
– Arbitrary Lagrangian–Eulerian formulation for body fitted moving grids;
– Embedded formulation for complex/dirty geometries;
– Edge-based data structures for speed;

– Optimal data structures for different supercomputer architectures;
– Bottom-up coding from the subroutine level to assure an open-ended, expandable architecture.

Fig. 2 continued
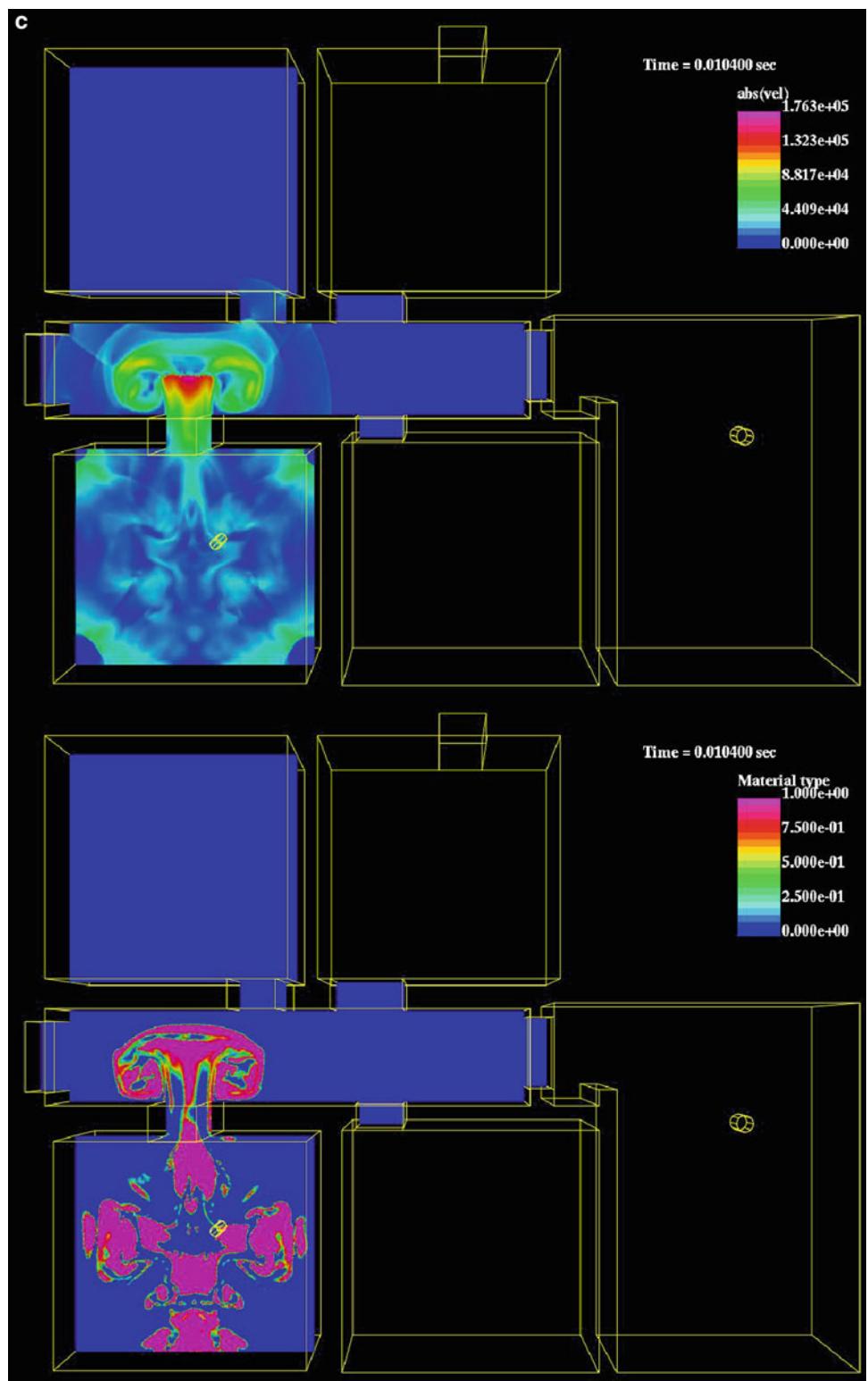
The code has had a long history of relevant applications [5–13]. Over the past 3 years, FEFLO has been ported to both shared memory [14–16] and distributed memory [7,17], and [18] machines.

The spatial approximation is accomplished via the Galerkin weighted residual method. The unknown vector $\mathbf{u} = [\rho, \rho u, e]$ is approximated by a set of shape-functions:

$$\mathbf{u} \approx N^i \mathbf{u}_i^h \tag{1}$$

where N^i denotes the shape function associated with node i and $\mathbf{u}_i^h$ the numerical value of $\mathbf{u}$ at node i. Weighing (1) with

Fig. 2 continued
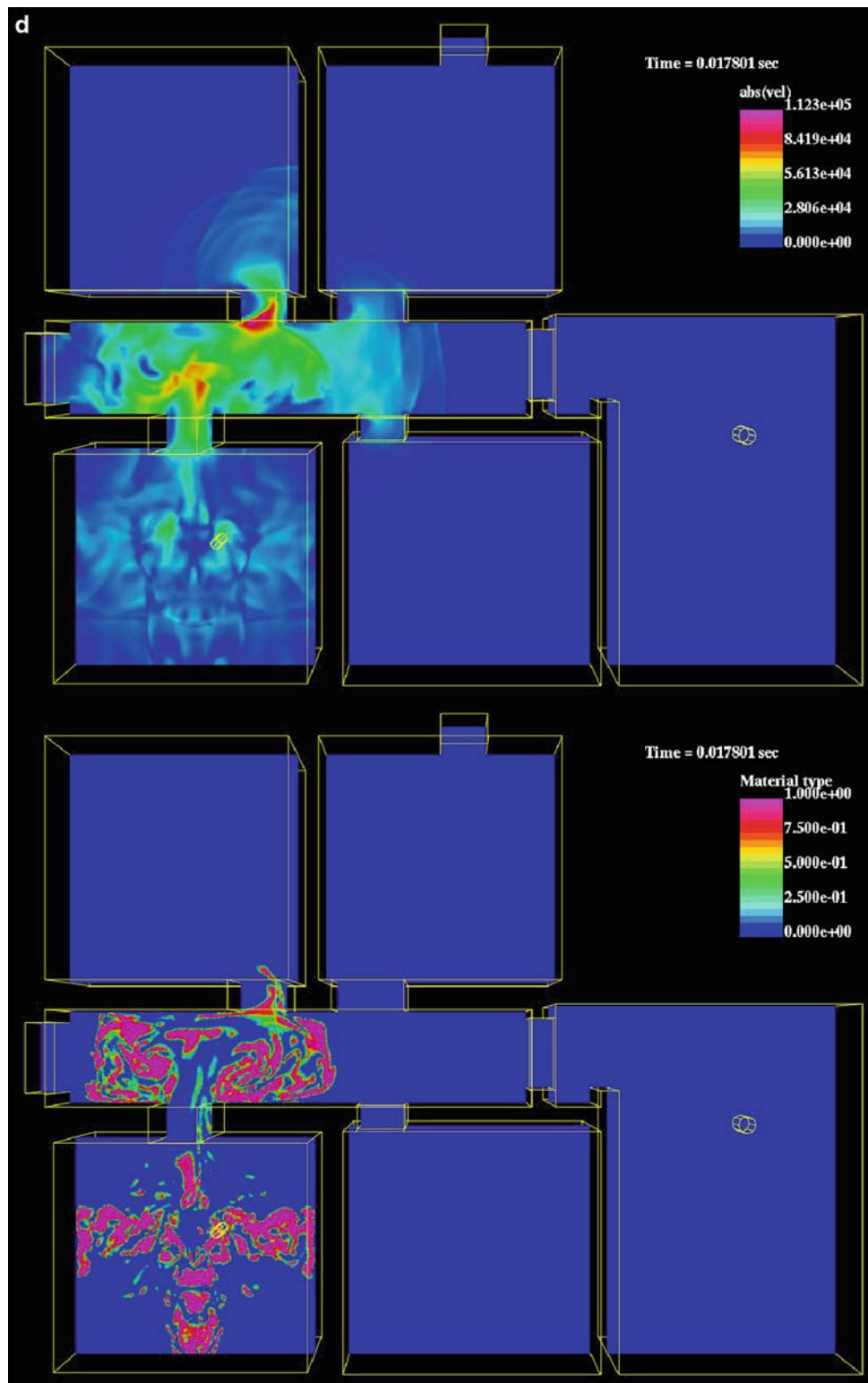
the available set of shape-function N^i leads to

$$\int_\Omega N^i \left(\mathbf{u}^h_{,t} + \nabla \cdot \mathbf{F} \right) d\Omega = 0 \Rightarrow \int_\Omega N^i \left[N^i(\hat{\mathbf{u}}_j)_{,t} \right.$$

$$\left. + \nabla \cdot \mathbf{F}(N^i \hat{\mathbf{u}}_j) \right] d\Omega = 0 \qquad (2)$$

where $\mathbf{F} = [\rho u, \rho u^2 + P, u(e + P)]$. In order to simplify the algebra (and CPU) involved, one may use, without noticeable deterioration of results

$$\mathbf{F}(N^j \hat{\mathbf{u}}_j) = N^j \mathbf{F}(\hat{\mathbf{u}}_j) \qquad (3)$$

Fig. 2 continued
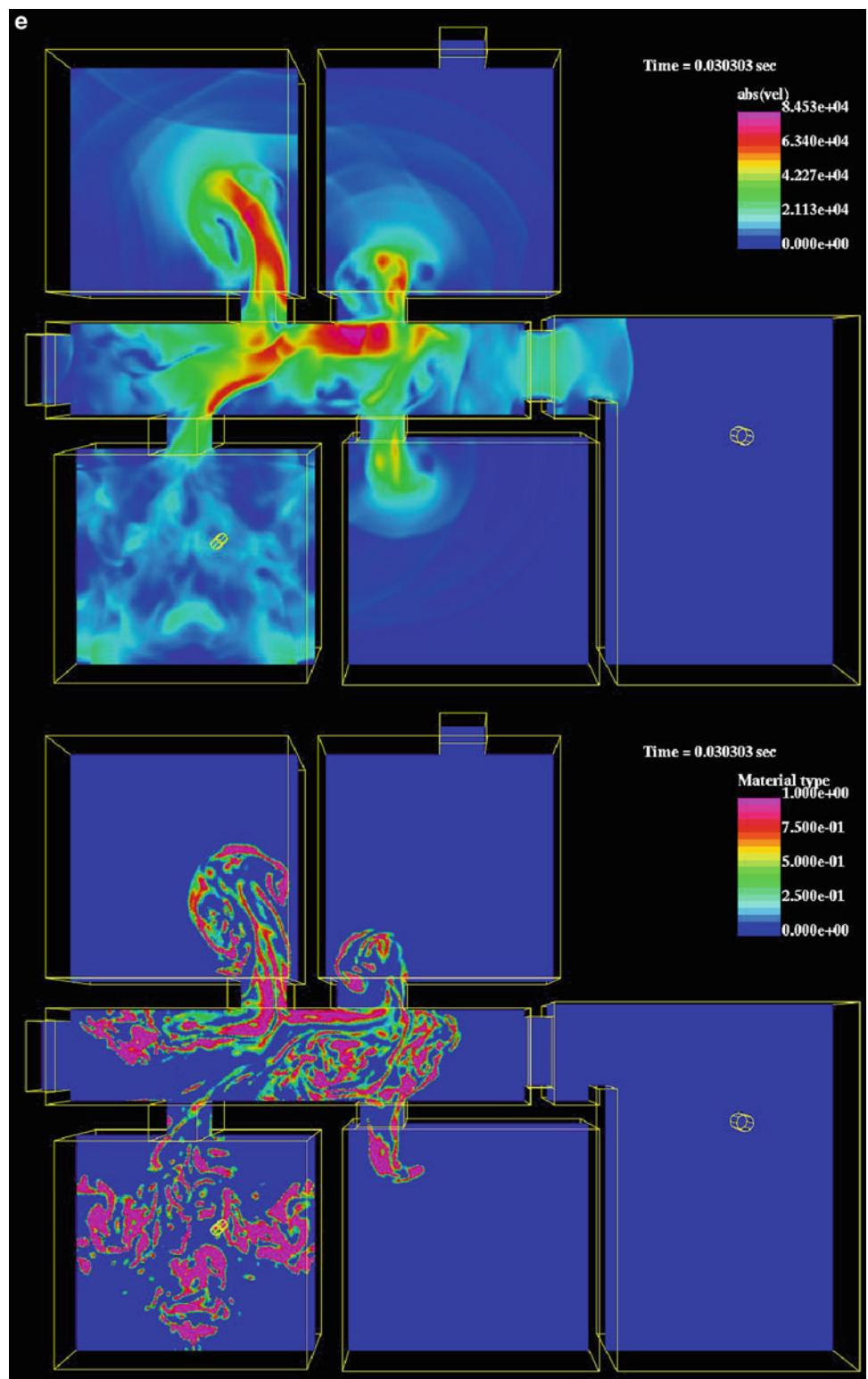
which then translates into

$$\int_\Omega N^i N^j \, \mathrm{d}\Omega \, (\hat{\mathbf{u}}_{\mathbf{j}})_{,t} + \int_\Omega N^i \nabla \cdot N^j \, \mathrm{d}\Omega \, \mathbf{F}(\hat{\mathbf{u}}_{\mathbf{j}}) = 0 \qquad (4)$$

or

$$\mathbf{M}_c \cdot \hat{\mathbf{u}}_{,t} = \mathbf{r}, \quad \mathbf{r} = \mathbf{r}(\mathbf{u}) \qquad (5)$$

Obviously, integration by parts is possible for (5). For linear elements, one can show that this is equivalent to a finite

Fig. 2 continued
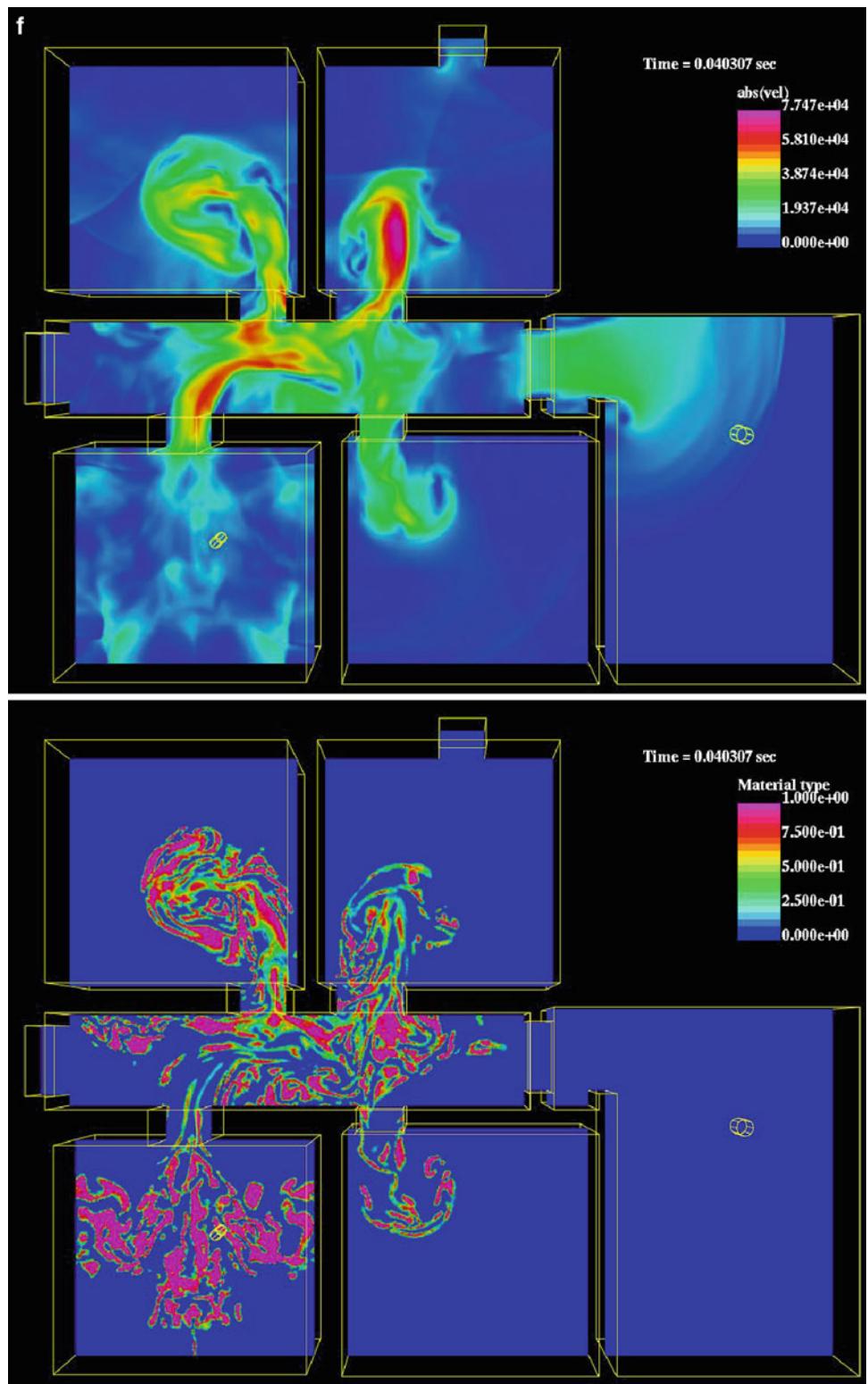
volume method. All appearing integrals are evaluated using the element subdomain paradigm:

$$\int_{\Omega} \cdot\cdot = \sum_{\text{el}} \int_{\Omega_{\text{el}}} \cdot\cdot \qquad (6)$$

For linear elements, it is advantageous to convert the element-based evaluations of (5) into an edge-based loop of the form:

$$\mathbf{r}^j = d_k^{ij} \left(\mathbf{F}_j^k + \mathbf{F}_i^k \right) \qquad (7)$$

Fig. 2 continued
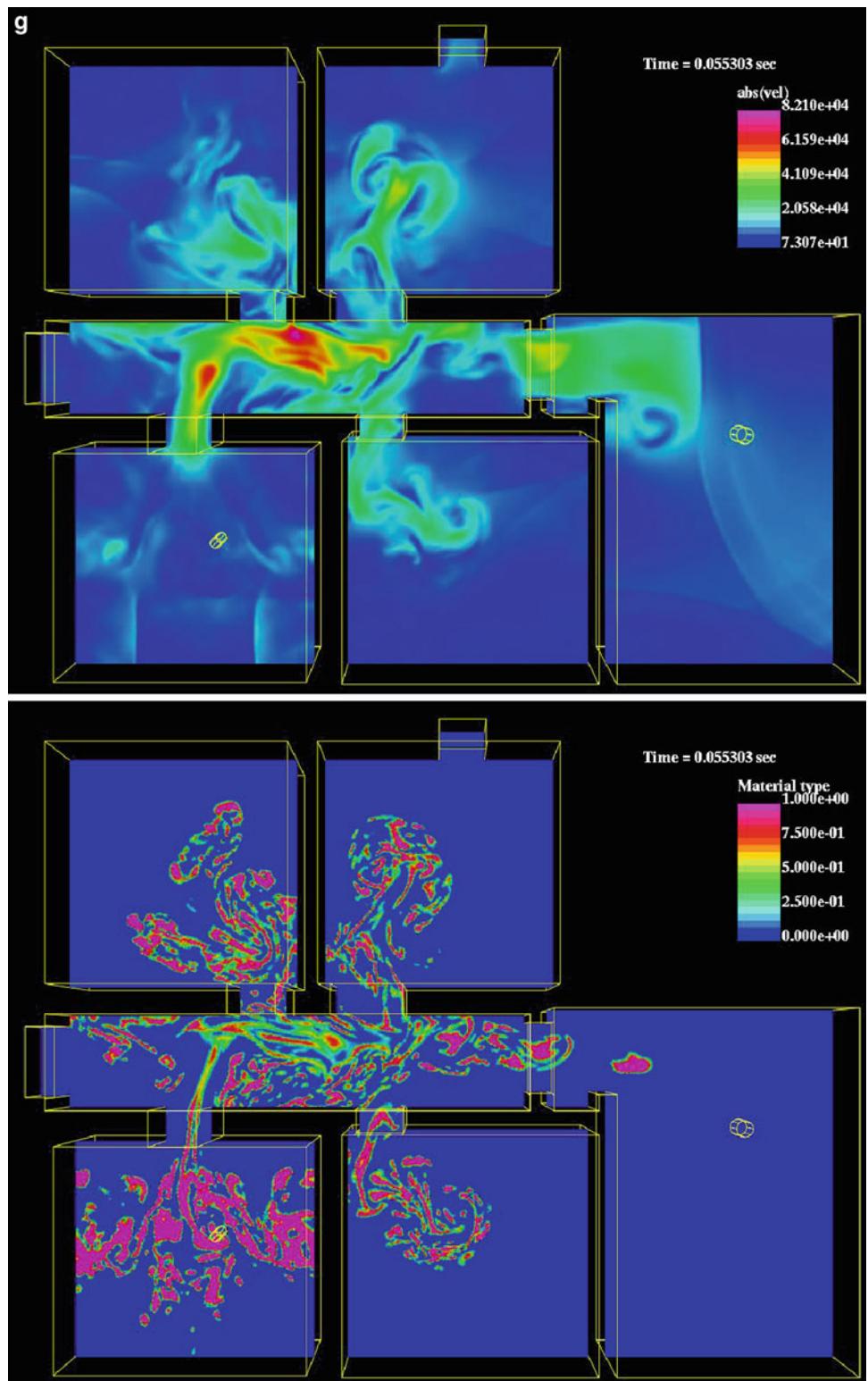
where d_k^{ij} contains all the geometric parameters associated with the elements surrounding the edge i, j and the dimension k. The inner product over the dimensions k may be written in compact form as

$$r^i = D^{ij}\mathbf{F}_{ij} = D^{ij}(f_i + f_j) \tag{8}$$

where the f_i are the 'fluxes along edges', obtained from the scalar product

$$f_i = S_k^{ij}\mathbf{F}_i^k, \quad S_k^{ij} = \frac{d_k^{ij}}{D^{ij}}, \quad D^{ij} = \sqrt{d_k^{ij}d_k^{ij}} \tag{9}$$

For the standard Galerkin approximation we have

Fig. 2 continued
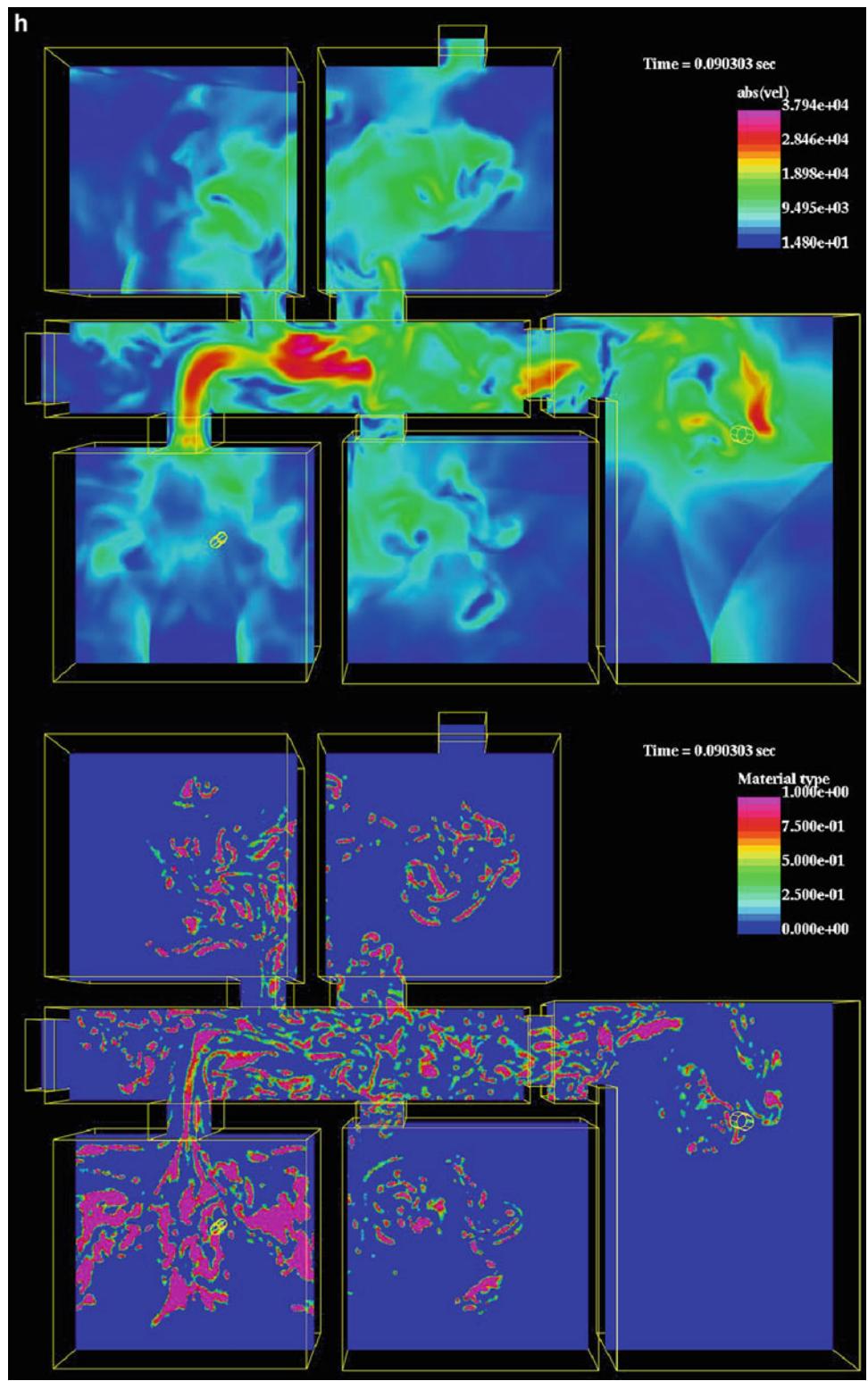
$$\boldsymbol{F}_{ij} = f_i + f_j \qquad (10)$$

Comparing this expression to a 1-D analysis, we see that it corresponds to a central difference approximation of the

first-order derivative fluxes. This flux is replaced by the consistent numerical flux described in the previous section.

The extrapolation to neighboring values required for limiting is accomplished by evaluating the gradients at the nodes [19].
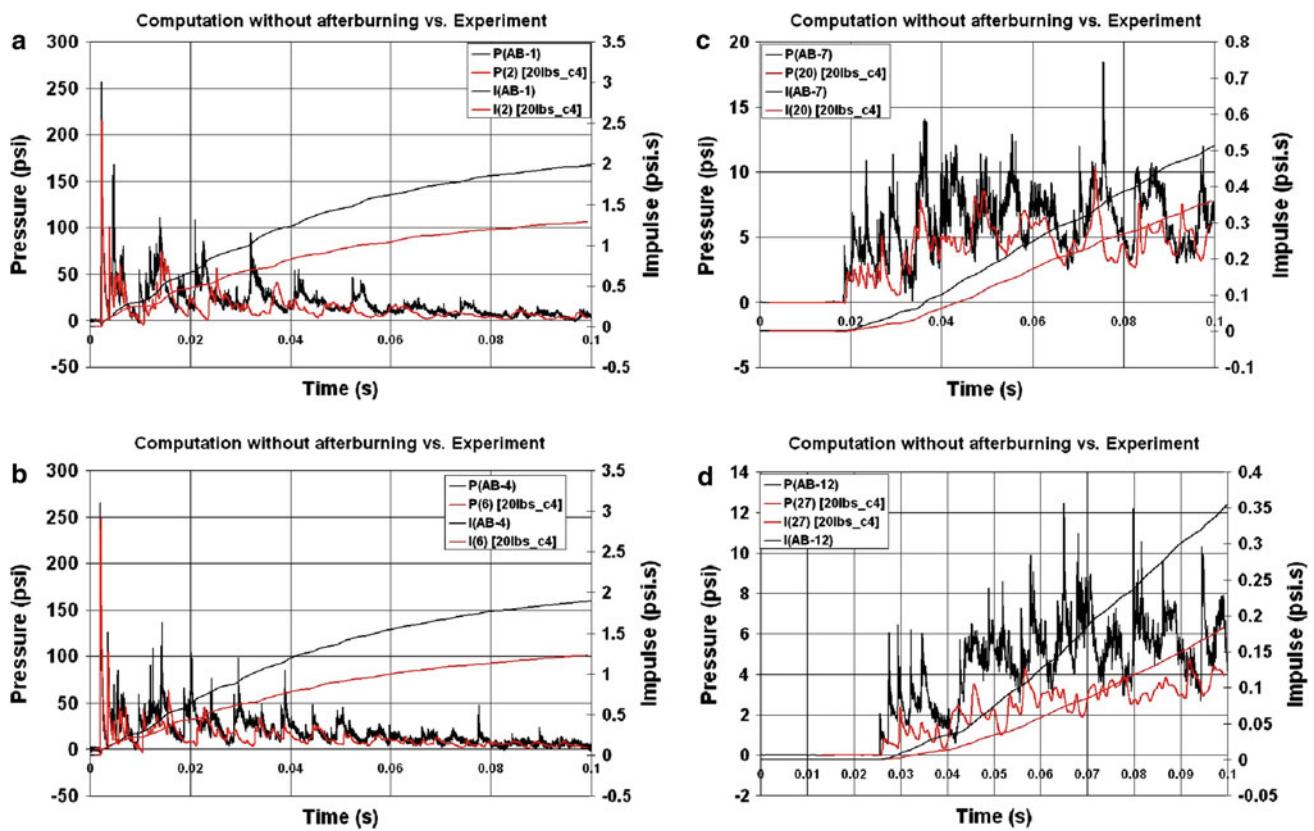
Fig. 3 **a, b** Comparison of measured and calculated pressure and impulse histories for an ideal explosive modeling (Gauges AB-1 and AB-4). **c, d** Comparison of measured and calculated pressure and impulse histories for an ideal explosive modeling (Gauges AB-7 and AB-12)

The governing equations in this study were 3-D the Euler equations. The JWL EOS [20] was used for the explosive part.

"Cheetah", a thermo-chemical code developed by LLNL [21], which solves the thermo-dynamic equation between product species to find chemical equilibrium, was used to estimate the remaining products after detonation. From these remaining species, the afterburning energy was computed and added to the flow field.

Afterburning modeling within numerical code is described into energy calculation term as follows:

$$\rho e^{n+1} = \rho e^n + \rho Q(\lambda^{n+1} - \lambda^n) \tag{11}$$

where Q denotes afterburning energy and λ is the burn coefficient. The burn coefficient is obtained as follows:

$$\lambda_{,t} = a \left(\frac{p}{p_0}\right)^{1/6} \sqrt{1 - \lambda} \tag{12}$$

where p denotes the pressure, p_0 is the ambient pressure and a is the afterburning coefficient. The estimate burn times is given $t_{\text{burn}} = \frac{2}{a}$, For a typical explosive, $a = 1,950$ is used.

The JWL EOS used in this study is as follows:

$$P_s = A \left(1 - \frac{\omega}{R_1 v}\right) \exp(-R_1 v)$$
$$+ B \left(1 - \frac{\omega}{R_2 v}\right) \exp(-R_2 v) + \frac{\omega E_s}{v} \tag{13}$$

3 Test facility modeling

The test facility was built by the Air Force Research Laboratory, Eglin Air Force Base. It consists of five distinct rooms inter connected by corridors and doorway as shown in Fig. 1. The entire facility is buried with tunnel access on the west and north side. Those accesses can be used to vent the gas products of the explosions. Extra venting circular holes are also present in room #3 (static detonation) and room #5. In order to measure pressures in five rooms, gauges have been installed. Six gauges installed on the wall in room #3 where the detonation occurs, three in the corridor, and one in the ceiling of the other rooms as shown in Fig. 1.

Table 1 Mole fraction of C-4 at frozen temperature (1,800 K) by Cheetah

Name	Phase	mol/kg	mol gas/mol explosive
N_2	Gas	1.206e+001	2.553e+000
CO	Gas	8.294e+000	1.756e+000
H_2O	Gas	6.185e+000	1.309e+000
CO_2	Gas	5.227e+000	1.106e+000
CH_4	Gas	4.224e+000	8.942e−001
H_2	Gas	1.513e+000	3.202e−001
NH_3	Gas	4.065e−001	8.604e−002
C_2H_6	Gas	1.082e−001	2.291e−002
CH_2O_2	Gas	6.632e−002	1.404e−002
C_2H_4	Gas	6.408e−002	1.357e−002
CHNO	Gas	4.944e−002	1.047e−002
CH_3OH	Gas	5.637e−003	1.193e−003
H_2Oa	Gas	3.178e−003	6.726e−004
HCN	Gas	2.492e−003	5.275e−004
C_2H_2	Gas	1.349e−003	2.856e−004
Acetone	Gas	2.358e−004	4.991e−005
C_2H_6o	Gas	1.595e−004	3.376e−005
NH_3a	Gas	1.111e−004	2.351e−005
H	Gas	2.196e−005	4.650e−006
NO	Gas	1.662e−007	3.518e−008
N_2O	Gas	8.192e−010	1.734e−010
O	Gas	5.101e−011	1.080e−011
N	Gas	2.008e−011	4.251e−012
O_2	Gas	6.958e−012	1.473e−012
NO_2	Gas	4.183e−014	8.854e−015
C	Gas	3.978e−016	8.421e−017
O_3	Gas	7.407e−024	1.568e−024
*C	Graphite	0.000e+000	0.000e+000
*C	Liquid2	0.000e+000	0.000e+000
*C	Liquid	0.000e+000	0.000e+000
*C	Diamond	0.000e+000	0.000e+000
Total gas		3.821e+001	8.089e+000
Total cond.		0.000e+000	0.000e+000

* denotes that the species are "liquid state or solid state", not "gaseous state"

4 Computed results

4.1 20 lb C-4 detonation without afterburning

The first explosive charge used was a C-4, about 20 lbs (9.072 kg), cylinder (bare charge) with a diameter of 4.5 in. (11.43 cm), and a length of 22.5 in. (57.15 cm). The charge was located at the center of the detonation room and was initiated from top center. The initial simulations used the standard ideal-explosive JWL–EOS [20]. Figure 2 shows the Gouraud shadings of computed absolute velocity and detonation product fraction from 0.5 to 90 ms. The propagation

of the shock waves throughout the facility is clearly depicted. To save CPU time, the simulation was divided into four phases. At the first phase, 3D simulation with the HE in a small domain was performed. The mesh resolution around the HE is about 1 cm/element. The result was interpolated onto a mesh encompassing the entire detonation room #3 as second phase as shown in Fig. 2a blue region. The simulation was stopped before the shock reached the doorway on the north. Phase three used a mesh covering room #3, room #1, and the corridor in Fig. 2b. The final phase was covering the entire facility as shown in Fig. 2d. The total computational elements are 60M elements for the whole domain.

Figure 3 shows comparisons of pressure/impulse time-history between the experimental data (black line) and our numerical calculations for an ideal explosive (i.e., without afterburning, depicted in red). The results for all stations within the detonation room (room #3) show very similar results: the long-term impulse (and hence, energy) and the late arrival of the waves indicate that the computed energy release under-estimates the measured data. This simulation was carried out prior to the experiments, to provide estimates for experimental gauge ranging. Here, the critical data of the initial shock peak pressure and time of arrival were required. For this purpose, the simulation provided very satisfactory data, as the two first peak pressures in room #3 were accurately calculated. However, the long-term calculated impulse values were lower than the measured values. Figure 3c and d show the pressure and impulse histories of gauges outside the detonation room. The simulation calculated fairly accurately the time of arrival of the first shock wave, but the second peak was delayed and the delay was increased as the distance from the blast room. Thus, for instance, Time-of-Arrival (TOA) of the second shock at AB-12 was significantly delayed: 27.5 ms in the experiment and 30 ms for the calculation. The lower impulse and delayed arrival of shocks were indicative of a lower energy contribution than measured. Further analysis indicated that estimated energy was approximately 10% lower than measured, in line in after-burn energy estimates. Thus, we have decided to include afterburn effects in the detonation model.

4.2 20 lb C-4 detonation with afterburning

First important issue to address is how much C, CO, or other burnable products remain after the detonation is completed. Cheetah [21] was adopted to estimate the frozen mass fractions. Cheetah is a thermo-chemical code developed by LLNL. It solves the thermo-dynamic equation between product species to compute a chemical equilibrium status and also calculates values such as CJ values, JWL parameters, etc. In this study the mass fraction at frozen temperature (about 1,800 K) was obtained by using Cheetah. Here, "frozen" means that the composition of the reactant gases is fixed at
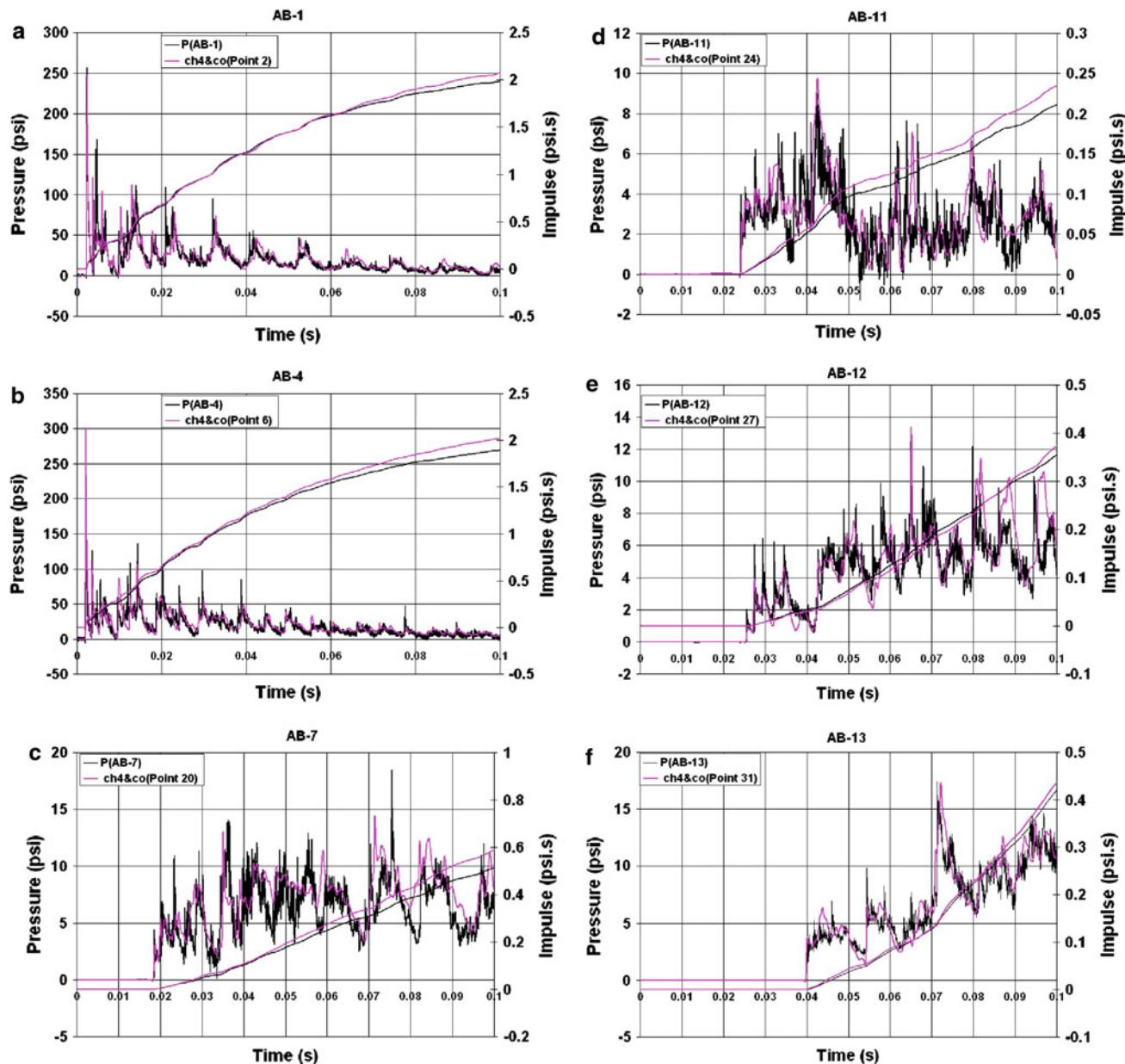
Fig. 4 a, **b** Comparison of measured and computed pressure and impulse histories for C-4, modeling afterburning (AB-1 and AB-4). **c**, **d** Comparison of measured and computed pressure and impulse histories for C-4, modeling afterburning (AB-7 and AB-11). **e**, **f** Comparison of measured and computed pressure and impulse histories for C-4, modeling afterburning (AB-12 and AB-13)

the freeze-out temperature from Cheetah manual [21]. The afterburning energy to be released was estimated from the results according to the following procedure.

The C-4 detonation product mass fraction along the explosive isentrope at frozen temperature (1,800 K) obtained from Cheetah is shown in Table 1. There are 22% of CO and 11% of CH_4. Likely CO and CH_4 reactions are $CO + 0.5O_2 = CO_2 + 281$ kJ/mol and $CH_4 + 2O_2 = CO_2 + 2H_2O + 802$ kJ/mol, respectively. The estimated total energy is 5,730 kJ/kg and will be released in 1 ms.

Based on the room dimensions, it contains 925 mol of O_2. Hence, there is enough oxygen to burn both CO and CH_4. The ignition temperatures are 853–923 K for CO, and 923–1,023 K for CH_4, respectively. Hence, afterburning may continue for a long time after detonation wave passage, as the temperature will remain high in the room for a long time.

Figure 4 shows comparisons of pressure and impulse histories between the measured and computed values that included afterburning. In Fig. 4, the black lines denote experimental data and the magenta line denote the numerical

results, which assume all CO and CH_4 to be burned. The computed results match the experimental results were far better than the previous (non-afterburn) results. The peak shock values and arrival times were in excellent agreement with experimental results for all rooms. The TOA of all following shocks has been improved considerably. Total estimated impulses agreed with experimental data too. Even for station point AB-13, which is located the farthest from the detonation point, the computations for several blast wave reverberations agree nicely with the experimental results, for both peak pressures and TOA, as well as total impulse.

4.3 16.7 lb AFX757 detonation

The second explosive used was AFX757. Again, a bare cylinder of about 16.7 lbs (7.575 kg) with a diameter of 4.0 in. (10.16 cm) and a length of 20.0 in. (50.8 cm), hung at the center of the room and top detonated. AFX757 includes 33% of Aluminum, so that afterburning is expected to add significantly more energy than for C-4. A calculation along the explosive isentrope was performed using "Cheetah" to obtain the mass fraction during the decomposition. In this study, we were researching the proper energy release during the long-term blast evolution limited in the small bare charges in large rooms. We used Cheetah to obtain the estimated energy after frozen temperature. So the Cheetah calculation was performed assuming all Al is burned inside detonation products to avoid the computation of the complicated kinetics of Al reactions.

As shown in Table 2, there are 57% of H_2, 18% of CO remaining for total gas product, and 45% of carbon graphite remaining for the solid product. Usually the frozen temperature in Cheetah is set to 1,800 K, but the calculation along the explosive isentrope gave the values at 1,662 K. So in this study, we set the frozen temperature to 1,662 K. Chemical reactions of these include $H_2 + 0.5O_2 = H_2O + 285.84$ kJ/mol, $CO + 0.5O_2 = CO_2 + 281$ kJ/mol, and C (graphite) $+ O_2 = CO_2 + 393.5$ kJ/mol, respectively. The estimated total energy is 7,734 kJ/kg.

The room size contains enough oxygen to burn the H_2, CO and the carbon graphite. The ignition temperature of H_2 is 853–873 K and that of graphite is around 1,000 K. In this study all three afterburning reactions were included.

Figure 5 shows comparisons of measured and computed pressure and impulse histories. Two data sets were shown for the computed results: with and without afterburning. In each figure, blue line denotes the experimental result, green line presents the computed results without afterburning (treating AFX757 as an ideal explosive with an estimated JWL–EOS, and magenta line presents the computed results that include afterburning. The computed results without afterburning matched well the first shock arrival time and the two first pressure peaks. Nevertheless, estimated long-

Table 2 Mole fraction of AFX757 at frozen temperature (1,662 K) by Cheetah

Name	Phase	mol/kg	mol gas/mol explosive
H_2	Gas	1.373e+001	8.101e−001
CO	Gas	4.357e+000	2.571e−001
N_2	Gas	2.997e+000	1.768e−001
HCl	Gas	2.553e+000	1.506e−001
HCN	Gas	7.565e−002	4.464e−003
CH_4	Gas	4.121e−002	2.432e−003
C_2H_2	Gas	2.157e−002	1.273e−003
P_2	Gas	2.562e−003	1.511e−004
H	Gas	1.841e−003	1.086e−004
C_2H_4	Gas	4.918e−004	2.902e−005
H_2O	Gas	3.475e−004	2.050e−005
Cl	Gas	2.406e−004	1.420e−005
NH_3	Gas	1.252e−004	7.387e−006
CO_2	Gas	3.334e−005	1.967e−006
P	Gas	1.754e−005	1.035e−006
C_2H_6	Gas	9.064e−007	5.348e−008
Al	Gas	6.204e−007	3.660e−008
CHNO	Gas	5.488e−007	3.238e−008
H_2Oa	Gas	2.063e−007	1.217e−008
Cl_2	Gas	1.249e−007	7.372e−009
NH_3a	Gas	3.898e−008	2.300e−009
CH_2Cl_2	Gas	2.034e−009	1.200e−010
CH_2O_2	Gas	3.494e−010	2.062e−011
CH_3OH	Gas	2.746e−010	1.620e−011
N	Gas	2.137e−011	1.261e−012
NO	Gas	1.920e−011	1.133e−012
C	Gas	4.805e−013	2.835e−014
O	Gas	2.386e−013	1.408e−014
$CHCl_3$	Gas	7.187e−014	4.240e−015
Acetone	Gas	2.350e−014	1.386e−015
C_2H_6o	Gas	1.614e−014	9.523e−016
CH_2Cl_2a	Gas	7.262e−016	4.285e−017
N_2o	Gas	3.742e−016	2.208e−017
O_2	Gas	2.728e−018	1.609e−019
CCl_4	Gas	2.846e−019	1.679e−020
O_6P_4	Gas	3.294e−021	1.943e−022
NO_2	Gas	4.644e−023	2.740e−024
O_3	Gas	8.088e−036	4.772e−037
*C	Graphite	6.578e+000	3.881e−001
*Al_2O_3	Solid	4.475e+000	2.640e−001
*Aln	b4-Solid	3.282e+000	1.936e−001
*$O_{10}P_4$	Solid	0.000e+000	0.000e+000
*P	Liquid-ii	0.000e+000	0.000e+000
*P	Liquid	0.000e+000	0.000e+000
*P	Solid-iii	0.000e+000	0.000e+000
*P	Solid-ii	0.000e+000	0.000e+000
*P	Solid-i	0.000e+000	0.000e+000

Table 2 continued

Name	Phase	mol/kg	mol gas/mol explosive
*Al_2O_3	Liquid	0.000e+000	0.000e+000
*Aln	b1-solid	0.000e+000	0.000e+000
*Al	Liquid	0.000e+000	0.000e+000
*Al	Solid	0.000e+000	0.000e+000
*C	Liquid2	0.000e+000	0.000e+000
*C	Liquid	0.000e+000	0.000e+000
*C	Diamond	0.000e+000	0.000e+000
Total gas		2.378e+001	1.403e+000
Total cond.		1.433e+001	8.458e−001

* denotes that the species are "liquid state or solid state", not "gaseous state"

term energy (and impulse) was quite low compared with the experimental results. On the other hand, the computed results with afterburning agreed nicely with the experimental results. The computed results were able to accurately match several pressure amplitudes peaks and TOA, and showed excellent agreement with the measures impulse. These results demonstrated that the afterburn model matched well not just the total energy released by the AFX757 detonation, but also the rate at which this energy was released through afterburning.

5 Conclusions

The numerical study of long-term blast wave evolution, initiated by detonating either C-4 or AFX757, in a confined multi-room test facility, was performed. The JWL EOS was used to model the detonation of the explosive. The computed results without considering afterburning could calculate very well the first blast wave time of arrival and the peak values for the first two reverberations. However, they could not predict well the impulse and the following shock waves (both time-of-arrival and peak pressures) during the long-term blast evolution. To improve the calculation accuracy, which obviously resulted from lower estimated energy release, the thermo chemical code "Cheetah" was used to estimate the burnable products after detonation. The Mole fractions of the burnable detonation products were calculated by Cheetah, and the estimated afterburning energy was added to the flow field. This procedure improved significantly the accuracy of the computed results. The computed results with afterburning were able to accurately match the TOA and peak pressure values for several blast wave reverberations, in all rooms of the facility. This methodology is limited to small bare charges in a large room, where plenty of Oxygen is available, but it is applicable to both a slightly underoxidized explosive like C-4, and a heavily aluminized
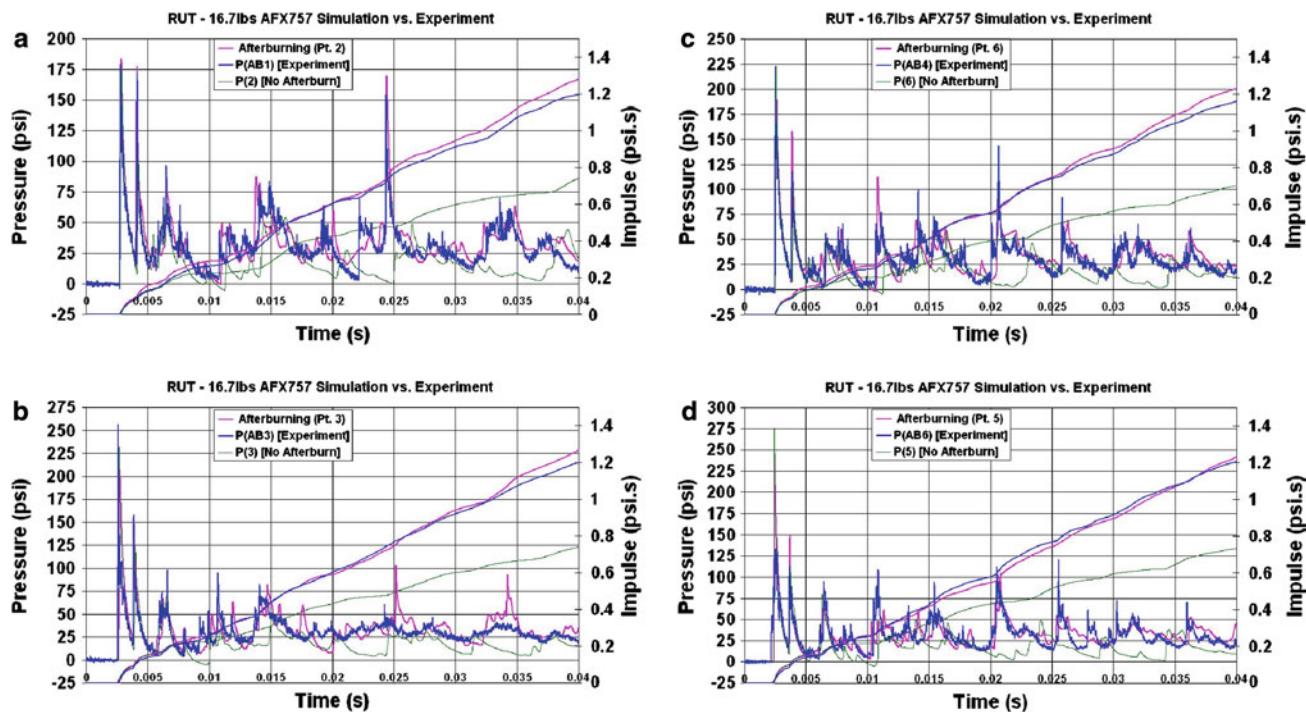

Fig. 5 a, **b** Comparison of measured (*blue*) and computed pressure and impulse histories for AFX757 without (*green*) and with (*magenta*) afterburning included (AB-1 and AB-3). **c**, **d** Comparison of measured (*blue*) and computed pressure and impulse histories for AFX757 without (*green*) and with (*magenta*) afterburning included (AB-4 and AB-6)

explosive such as AFX757. These results demonstrated that the afterburn model matched well not just the total energy released by the detonation, but also the rate at which this energy is released through afterburning.

References

1. Souers, P.C., Wu, B., Haselman, L.C., Jr.: Detonation Equation of State at LLNL, 1995. In: Energetic Materials Center Lawrence Livermore National Laboratory, 1 February (1996)
2. Cooper, P.W., Kurowski, S.R.: Introduction to the Technology of Explosives. Wiley-VCH (1996)
3. Schwer, D., Kailasanath, K.: Blast Mitigation by Water Mist (1) Simulation of Confined Blast Waves. NRL/MR/6410-02-8636
4. Kuhl, A.L., Forbes, J., Chandler, J., Oppenheim, A.K., Spektor, R., Ferguson, R.E.: Confined combustion of TNT explosion products in air. UCRL-JC-131748
5. Baum, J.D., Löhner, R.: Numerical simulation of shock interaction with a modern main battle field tank. AIAA-91-1666 (1991)
6. Baum, J.D., Luo, H., Löhner, R.: Numerical Simulation of a Blast Inside a Boeing 747. AIAA-93-3091 (1993)
7. Ramamurti, R., Löhner, R.: Simulation of flow past complex geometries using a parallel implicit incompressible flow solver. In: Proc.11th AIAA CFD Conf., pp. 1049, 1050, Orlando, FL, July 1993
8. Baum, J.D., Luo H., Löhner, R.: A new ALE adaptive unstructured methodology for the simulation of moving bodies. AIAA-94-0414 (1994)
9. Baum, J.D., Luo H., Löhner, R.: Numerical simulation of blast in the world trade center. AIAA-95-0085 (1995)
10. Baum, J.D., Luo, H., Löhner, R., Yang, C., Pelessone, D., Charman, C.: A coupled fluid/structure modeling of shock interaction with a truck. AIAA-96-0795 (1996)
11. Baum, J.D., Löhner, R., Marquette T.J., Luo, H.: Numerical simulation of aircraft canopy trajectory. AIAA-97-1885 (1997)
12. Baum, J.D., Luo, H., Mestreau, E., Löhner, R., Pelessone, D., Charman, C.: A coupled CFD/CSD methodology for modeling weapon detonation and fragmentation. AIAA-99-0794 (1999)
13. Ramamurti, R., Sandberg, W., Löhner, R.: Simulation of flow about flapping airfoils using a finite element incompressible flow solver. AIAA-99-0652 (1999)
14. Löhner, R.: Renumbering strategies for unstructured-grid solvers operating on shared-memory, cache-based parallel machines. Comput. Methods Appl. Mech. Eng. **163**, 95–109 (1998)
15. Tuszynski, J., Löhner, R.: Parallelizing the construction of indirect access arrays for shared-memory machines. Commun. Appl. Numer. Methods Eng. **14**, 773–781 (1998)
16. Sharov, D., Luo, H., Baum J.D., Löhner, R.: Immentation of unstructured grid GMRES+LU-SGS method on shared-memory, cache-based parallel computers. AIAA-00-0927 (2000)
17. Löhner, R., Ramamurti, R.: A load balancing algorithm for unstructured grids. Comput. Fluid Dyn. **5**, 39–58 (1995)
18. Ramamurti, R., Löhner, R.: A parallel implicit incompressible flow solver using unstructured meshes. Comput. Fluids **5**, 119–132 (1996)
19. Löhner, R.: Applied CFD Techniques. Wiley, New York (2001)
20. Dobratz, B.M., Crawford, P.C.: Properties of chemical explosives and explosive simulants. In: LLNL Explosives Handbook
21. Fried, L.E., et al.: Cheetah 4.0 User's manual. LLNL (2004)